applied sciences

MDPI

Article

Numerical Simulation and Modeling of Mechano–Electro–Thermal Behavior of Electrical Contact Using COMSOL Multiphysics

Andrei Andras [1,*], Florin Dumitru Popescu [1,*], Sorin Mihai Radu [1], Dragos Pasculescu [2], Ildiko Brinas [1], Mirela Ancuta Radu [3] and Daniela (Furdui) Peagu [4]

[1] Department of Mechanical, Industrial and Transport Engineering (IMIT), University of Petroșani, 332006 Petroșani, Romania; sorin_mihai_radu@yahoo.com (S.M.R.); kerteszildiko@ymail.com (I.B.)
[2] Department of Automatics, Computers, Electrical and Energetics Engineering (ACIEE), University of Petroșani, 332006 Petroșani, Romania; dragospasculescu@upet.ro
[3] National Institute of Research and Development for Safety in Mines and Explosion Protection—INSEMEX Petrosani, 332047 Petrosani, Romania; mirela.radu@insemex.ro
[4] Doctoral School in Mines, Oil and Gases, University of Petrosani, 332006 Petrosani, Romania; danafurdui2012@yahoo.com
* Correspondence: andrei.andras@gmail.com (A.A.); fpopescu@gmail.com (F.D.P.)

Abstract: Electrical contacts are important circuit components with diverse industrial applications, and their failure can lead to multiple unwanted effects. Hence, the behavior of electrical contacts is a widely studied topic in the scientific literature based on various approaches, tools, and techniques. The present study proposes a new approach to numerical modeling and simulation based on the Holm contact theory, aiming to study the dependence between the electric potential and the temperature within an electrical contact. Structured in five sections, the research was conducted using COMSOL Multiphysics software (version 5.3) and its solid-state mechanics, electric current, and heat transfer modules in order to highlight contact behavior from mechanical, electrical and thermal points of view: the von Mises stress, contact force, electric field amplitude, variation of the electrical potential along the current path, temperature gradient, and dependence of temperature along the contact elements edges were obtained by simulation, and are graphically represented. The results show that the temperature increase follows a parabolic curve, and that for values higher than 4 mV of voltage drop, the temperature of the contact increases to 79.25 degrees (and up to 123.81 degrees for 5 mV) over the ambient temperature, thus the integrity of insulation can be compromised. These values are close (10–12%) to the analytically calculated ones, and also in line with research assessed in the literature review.

Keywords: electrical contact; joule heating; Thomson effect; simulation; COMSOL Multiphysics; current density; electrical contact temperature

check for updates

Citation: Andras, A.; Popescu, F.D.; Radu, S.M.; Pasculescu, D.; Brinas, I.; Radu, M.A.; Peagu, D. Numerical Simulation and Modeling of Mechano–Electro–Thermal Behavior of Electrical Contact Using COMSOL Multiphysics. *Appl. Sci.* **2024**, *14*, 4026. https://doi.org/10.3390/app14104026

Academic Editors: Jorge Bañuelos Prieto and Yanbo Wang

Received: 21 March 2024
Revised: 26 April 2024
Accepted: 8 May 2024
Published: 9 May 2024

Copyright: © 2024 by the authors. Licensee MDPI, Basel, Switzerland. This article is an open access article distributed under the terms and conditions of the Creative Commons Attribution (CC BY) license (https://creativecommons.org/licenses/by/4.0/).

1. Introduction

Electrical contacts are crucial circuit components present in most electric devices, such as relays, switches, breakers, connectors, breakers and integrated circuits. The theory and analysis of electrical contacts [1–5] is a multidisciplinary issue since it involves electrical, mechanical and thermal concepts, all aimed at understanding and improving the performance of these electrical connections used in various applications.

A contact system always consists of a pair of electric contacts and a source of contact force [6], with each contact made of conductive material, usually metal or metallic alloys. When a pair of contacts touch, electrical current passes with a certain electrical contact resistance. There are several factors [7] that influence the current flow and thus this resistance: contact area [8], shape [9], roughness [10], oxidation and coatings [11,12],

mechanical loads [13], etc. The electrical contacts' resistance should be low and stable, since its increase leads to contact failure and very high Joule heat losses [14].

The typical failure modes for electrical contacts consist of: (a) temperature increase in the contact area producing melting or quick aging, (b) elevated electrical contact resistance caused by fretting wear or oxidation, and (c) excessively small or large closing/opening forces.

Failures of electrical contacts and the causes leading to them are extensively studied in the scientific literature, based on several different analysis approaches.

First, there are theoretical analyses based on model types such as the single-point (or Holm tube) contact model [15,16], the multi-point contact model [17,18], and the fractal geometry theory model [19–21]. Several other scholars have used analytical models to study electrical contact behavior, with the authors of [22] presenting a study built on the improved elastic rough surface model, [23] introducing a new analytical model for the analysis of switching devices' contact areas for different voltage and current magnitudes, and [24] proposing a semi-analytical model based on the single asperity concept to highlight the flow of current between two contacting surfaces.

Next, electrical contacts have also been widely studied using experimental setups and measurements, employing a combined analytical and experimental investigation [25] to describe the electrical–thermal behavior of electrical contact systems, using a low-cost tabletop indenter setup [26] to measure the in-situ electrical contact resistance, determining experimentally the adhesion force and energy at contact interfaces for conductive, isotropic, and rough surfaces [27]. High-current automotive connectors were tested [28] to assess their thermal performance, experimental observations on contact resistance were summed up [29] to be used as an electrical contact guide, two distinct techniques were used during investigations [30] for different pressures, temperatures, and contact types, and trials were conducted [31] on copper/brass plug-and-sockets types of contacts.

Finally, there is the vast array of numerical methods. These started several decades ago with finite elements discretization [32,33] and solving in codes like FEAP [34–36] or discrete elements simulations using the LMGC90 open platform or MULTICOR software [37–40], but in recent years the continuous advancement of computer technology and the leaps in performance and processing power have allowed us to model, analyze, optimize and solve more and more complex problems of electrical contact systems. Nowadays, the numerical methods use dedicated engineering computer software, and are based on various techniques such as the boundary element method (BEM) [41–43], finite element method (FEM) [44–46] and coupled/multiphysics methods [47–50] to model and simulate contact behavior.

Angadi et al. [51] and other scholars reviewed and presented several forms of computer software available to researchers for the analysis of electrical contacts and their behavior, with MSC Marc, ANSYS, ABAQUS and COMSOL being the most used ones as subsequently detailed:

(a) MSC Marc software was used in [52] to create the model of an electric contact and compute the temperature distribution of joule heating compared with experimental results. The performance of pin and socket electrical contacts was assessed in [53] using a computer model also developed in MSC Marc software and numerical simulation;
(b) ANSYS was used by Duan et al. [54] to develop a coupled mechanical–electrical–thermal model, in order to prove the relation between electric contact shrink range, contact resistance and maximum stress, while also considering the temperature. The authors of [55] proposed a multi-physics model developed in ANSYS to investigate the thermal behavior of an electrical contact with a rough surface in two scenarios—direct and load transfer. The model developed and introduced in [56] combines ANSYS with a MATLAB code to accurately predict the contact forces, thermal contact resistance, surface separation and ECR, and provide an efficient tool to study electrical contact behavior from electrical, thermal and structural perspectives;

(c) The ABAQUS and FE-SAFE software types are both used [57] to numerically investigate and assess in detail the behavior of aviation electrical contacts. The authors of [58] used an ABAQUS-developed thermal–electric coupled simulation to study the contact pair insertion force and obtain the contact resistance. An analysis was conducted using a new electro-thermo-mechanical contact model developed by [59] in ABAQUS and two user-defined subroutines to show how the contact state significantly influences the local heating;

(d) Finally, the Swedish COMSOL Multiphysics software was used by Zhang et al. [60] to introduce a new fluid–solid heat transfer model coupled with contact mechanics and the thermo-electric effect, in order to highlight the importance of pressure to the failure of an electrical contact. Another COMSOL-developed model was proposed in [61] to conduct research on contact temperature characteristics and thus improve the performance of electrical contacts. The authors of [62] investigated, by simulation in COMSOL, the effects of the electric current and contact force on the temperature and resistance of a spring-type electrical contact.

However, regardless of the method applied or the software, used all have both limitations and advantages, so at this point there is no imposed standard requiring that a particular computer program or method of analysis be used. Taking this into consideration, given the extensive literature review pointing to the available software tools, and considering the experience and previous approaches [63–66] of the same research team involved in solving various engineering tasks using numeric simulation, in the present study, COMSOL software [67] was chosen for the analysis and SolidWorks for the creation of the geometric model.

Although it is obvious that there is a vast amount of research on electrical contacts using various approaches and techniques, as described and summarized in the literature review section, the general outcomes of any of these studies—whether they are mechanical, electrical, thermal, or coupled—share a single important common scope: finding the causes leading to electrical contact failures. Regardless of where these contacts are used, and to what currents, contact forces or mechanical stresses they are subjected, it is of utmost importance to fully understand their behavior under different scenarios, in order to improve their performance and avoid the hazards produced by underperforming or failing contacts.

In this paper, a new modeling approach based on Holm electrical contact theory was proposed, with the purpose being to investigate the dependance between the electric potential and the temperature of the electrical contact via numerical methods using the COMSOL software and FEM. Several simulations were conducted for different values of the electric potential difference to obtain the corresponding contact temperature. The results show that the temperature increase has a parabolic shape, and that for values of the voltage drop that are higher than 4 mV, the contact temperature increases by 79.25 degrees and more over the ambient temperature. These values are close (10–12%) to those calculated analytically, and are also in line with research addressed in the literature review. These values of temperature can compromise the integrity and performance of contact insulation, leading to potentially unwanted effects.

The paper is structured as follows: Section 1 introduces the purpose of the paper and presents a comprehensive literature review related to the studied themes. Section 2 presents the theoretical aspects regarding electric contacts. Section 3 shows the initial geometric model developed using SolidWorks software, followed by the step-by-step creation of the COMSOL model and the simulation studies run in the same software, and Section 4 discusses the results obtained.

2. Theoretical Considerations about Electrical Contacts

As described in the Introduction section, an electrical contact consists of a pair of usually metallic contact elements, by the touch of which conduction in an electrical circuit is established. In practice, the touching of the two elements is achieved by pressing one

element against the other by means of a force. This contact force can be produced by either springs (by compression or stretching) or bolts that mechanically join the two elements.

In contacts with a large area, the effective contact area is smaller as compared to the apparent touching area, because surfaces that appear smooth at real scale are actually rough and contaminated at the microscopic scale [68].

No matter how finely the contact surfaces are polished, the actual touch is achieved only in certain areas called contact points, where the current lines of flow are bent and undergo a constriction as shown in Figure 1. These micro-points of contact, which are grouped into contact areas, are called contact spots or a-spots, where the material is deformed. If the area of contact points A_F on which the contact force F is exerted is only a tiny fraction (0.01–0.05) of the apparent area A_a, there is a surface contact, as illustrated in Figure 2, where contact is achieved through three a-spots, noted as 1, 2, and 3.

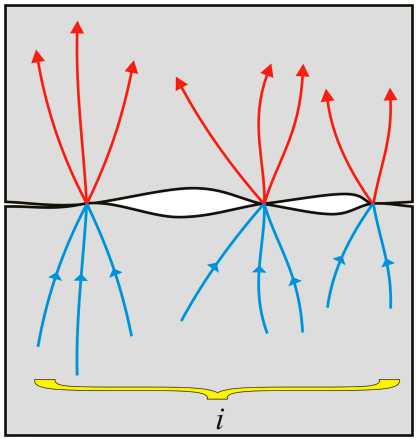

Figure 1. Constriction of the current lines of flow.

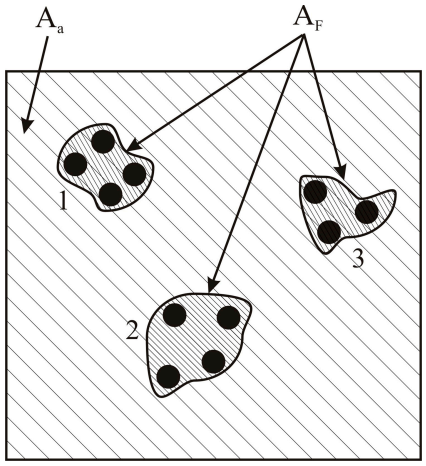

Figure 2. Surface contact illustration of effective and actual contact areas.

Each contact spot consists of micro-areas where the material is deformed either plastically, elastically or both. The dependence between the contact force F and the contact area A_F on which this force is exerted under plastic deformation conditions can be expressed using the formula of Holm [69]:

$$A_F = \frac{F}{\xi \cdot H} = n \cdot \pi \cdot a^2 \quad (1)$$

where a is the radius of the equivalent circle for each of the n contact zones.

For the calculation of the constriction resistance, two models can be applied [70], namely, the infinite conductivity sphere model and the flattened ellipsoid model.

2.1. The Model of the Infinite Conductivity Sphere

The model of the infinite conductivity sphere is shown in Figure 3.

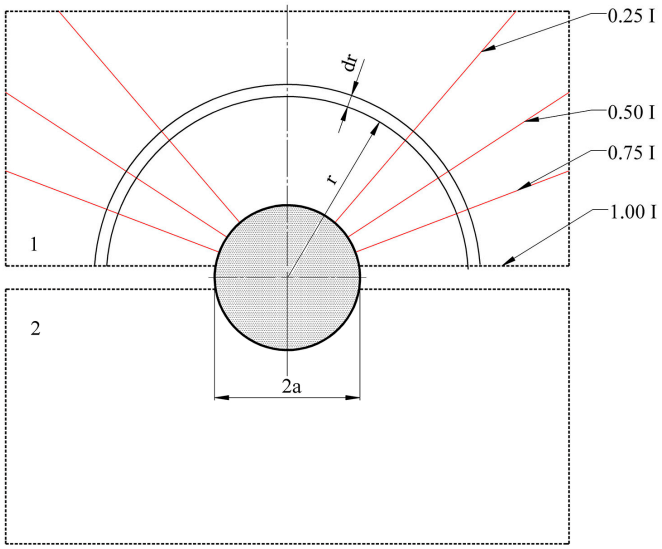

Figure 3. The model of the infinite conductivity sphere.

It consists of two half-spaces 1 and 2 of finite conductivity, which model the contact elements, where the electrical conduction is established by means of a sphere of radius a and infinite conductivity. The current lines are radial, and the equipotential surfaces are spherical. The current density is constant over the surface of a sphere of radius r.

If ρ is the resistivity of the material of the half-spaces, the elementary resistance is:

$$dR_s = \frac{\rho dr}{2\pi r^2} \tag{2}$$

and by integration, the constriction resistance of one half-space becomes:

$$R_s = \frac{\rho}{\pi}\int_a^\infty \frac{dr}{r^2} = \frac{\rho}{2\pi a} \tag{3}$$

The total contact constriction resistance of the two half-spaces in touch with the infinite conductivity sphere having a diameter $2a$ is twice the value given by Equation (3), i.e.,

$$R = \frac{\rho}{\pi a} \tag{4}$$

2.2. The Flattened Ellipsoid Model

In the case of the flattened ellipsoid model, the half-spaces 1 and 2 of finite conductivity are touching by means of a flattened ellipsoid, as shown in Figure 4. The equipotential surfaces are confocal ellipsoids, with the flattened ellipsoid as their base ellipsoid. To calculate the electrical resistance between the equipotential surface of the base ellipsoid (as a place of contact) and the surface of another equipotential confocal ellipsoid, formal analogy is used, which exists between the formulae characterizing the stationary electric field of direct current in a conducting medium and the formulae characterizing the electric field in an uncharged dielectric.

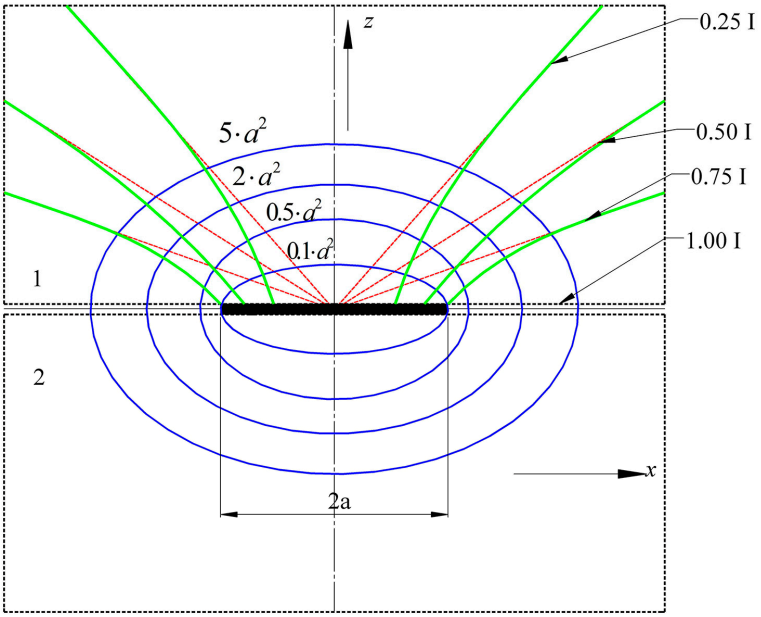

Figure 4. The flattened ellipsoid model.

In this case, the expression of striction conductance is identical to the expression of capacitance, in which permittivity ε is replaced by conductivity σ. Solving the problem in this way is possible assuming the same boundary conditions are allowed for both the conductive medium with conductivity σ and the dielectric medium with permittivity ε. Thus, both the base ellipsoid and the medium delimiting the surface of the confocal ellipsoid are assumed to have infinite conductivity, and the conductive medium between the surfaces of the ellipsoids has constant conductivity σ. Only in this case are the surfaces of the two ellipsoids equipotential surfaces in the stationary electric field, and the current lines are orthogonal to the surfaces of the ellipsoids.

If it is considered that the base ellipsoid is flattened, as in Figure 4, and that the contact surface is an ellipse, then the equipotential surfaces in the contact members are semi-ellipsoids, with the equation:

$$\frac{x^2}{\alpha^2+\mu}+\frac{y^2}{\beta^2+\mu}+\frac{z^2}{\mu}=1 \tag{5}$$

where α and β are the semi-axes of the flattened base ellipsoid in the plane xy. Confocal ellipsoids are defined by the parameter μ (μ = 0.1· a^2, μ = 0.5 · a^2, μ = 2 · a^2, μ = 5 · a^2,. . .). Thus, the semi-axes are: $\sqrt{\alpha^2+\mu}$ on axis x, $\sqrt{\beta^2+\mu}$ on axis y, and $\sqrt{\mu}$ on axis z.

The constriction resistance between the base semi-ellipsoid and a random confocal semi-ellipsoid is:

$$R_s=\frac{1}{4\pi\sigma}\int_0^{\mu}\frac{d\mu}{\sqrt{(\alpha^2+\mu)\left(\beta^2+\mu\right)\mu}} \tag{6}$$

If it is admitted that the contact ellipse is actually a circle, meaning that α = β = a, then the elliptical integral becomes a simple transcendent integral, and

$$R_s=\frac{1}{4\pi\sigma}\int_0^{\mu}\frac{d\mu}{(a^2+\mu)\sqrt{\mu}} \tag{7}$$

With the variable changes $\sqrt{\mu} = z$, $\mu = z^2$, and $\mathrm{d}\,\mu = 2z\,\mathrm{d}z$, we obtain

$$R_s = \frac{1}{2\pi\sigma}\int_0^{\sqrt{\mu}} \frac{\mathrm{d}z}{a^2+z^2} = \frac{1}{2\pi\sigma a^2}\int_0^{\sqrt{\mu}} \frac{\mathrm{d}z}{1+\left(\frac{z}{a}\right)^2} \tag{8}$$

With a new variable change $\frac{z}{a} = u$, and $\mathrm{d}\,z = a \cdot \mathrm{d}u$, we obtain

$$R_s = \frac{1}{2\pi\sigma a}\int_0^{\frac{\sqrt{\mu}}{a}} \frac{\mathrm{d}u}{1+u^2} = \frac{\rho}{2\pi a}\arctan\left(\frac{\sqrt{\mu}}{a}\right) \tag{9}$$

If instead of an ellipsoid a semi-space is considered, then $\mu \to \infty$, and Equation (9) becomes:

$$R_s = \frac{\rho}{4a} \tag{10}$$

The total constriction resistance is twice as high as R_s, that is,

$$R = \frac{\rho}{2a} \tag{11}$$

According to Holm [69], the current density across a flattened ellipsoid contact area can be approximated as

$$J(r) = \frac{i}{2\pi a} \cdot \frac{1}{\sqrt{a^2 - r^2}} \tag{12}$$

2.3. The Thermal Regime of Electrical Contacts

From the point of view of the thermal regime of electrical contacts, electric current passing through a contact causes the development of heat (Joule effect) because of contact resistance. In permanent thermal regime, the overtemperature due to contact resistance must be maintained within relatively low limits of 2–10 degrees, whereas in short-term thermal regimes such as a short circuit, the overheating must not lead to the melting of the contact elements. The study of thermal behavior is carried out for closed contacts, as if the contact elements are separated, additional physical processes such as arcing and material migration occur.

Figure 5 shows a contact point in whose touching area a number of m flow lines (tubes) of current i converge, such that the total current in the touch area is $I = \mathrm{m} \cdot i$. Figure 6 schematically details such a tube of current, which in the contact point covers the area ΔA_0.

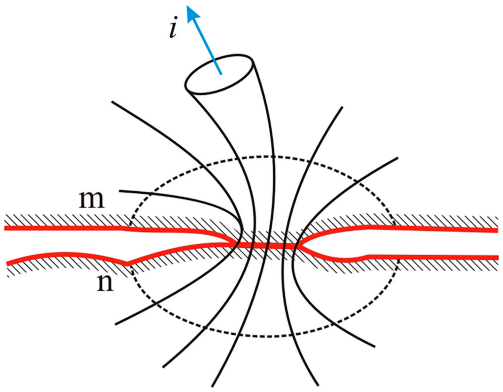

Figure 5. Contact point with converging flow lines (tubes) of current.

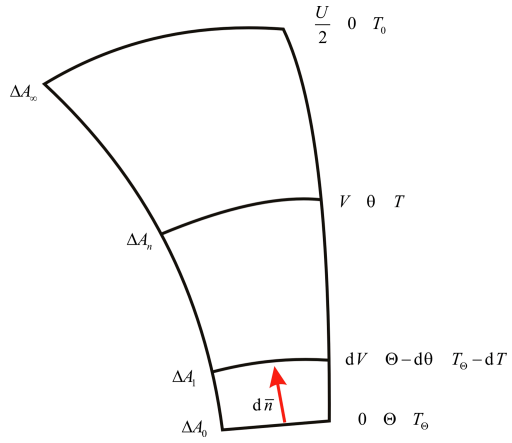

Figure 6. Detailed view of a tube of current.

Calculations are made with the following assumptions:

- The thermal flux developed in a certain current tube is transmitted outwards only through that current tube. There is no heat transfer between adjacent points m and n in Figure 5, which are assumed to be at the same temperature;
- The highest overtemperature is at the ΔA_0 surface, which also defines an isothermal surface, as a result of which the greatest restriction is located in the contact zone;
- The contact elements are made of the same homogeneous and isotropic material.

By the passing of current i through a current tube, equipotential and isothermal surfaces are defined as shown in Figure 6, considering the surface ΔA_2 with the reference parameters in terms of electric potential $V = 0$, overtemperature $\theta = \Theta$, and absolute temperature $T = T_\Theta$. A surface ΔA_n located far away, theoretically at a point infinitely far, is characterized by $V = U/2$, where U is the voltage on the contact, $\theta = 0$ and $T = T_0$.

One can see that the equipotential surfaces are also isothermal, due to the fact that equal thermal fluxes go through equal thermal resistances. Thus, the equations of electrical resistance R and thermal resistances R_t, for a segment of the current tube between the base surface ΔA_0 and the equipotential surface ΔA_1 situated at a distance d n from ΔA_0, are:

$$\mathrm{d}R = \frac{\mathrm{d}n}{\sigma \cdot \Delta\overline{A}_{01}} \tag{13}$$

$$\mathrm{d}R_t = \frac{\mathrm{d}n}{\lambda \cdot \Delta\overline{A}_{01}} \tag{14}$$

where $\Delta\overline{A}_{01}$ represents an average value of the area over the distance dn; σ is the electrical conductivity; λ is the thermal conductivity.

For the elementary temperature variation, the equation of Fourier is valid when written in the form

$$\mathrm{d}T = -P_t \cdot \mathrm{d}R_t \tag{15}$$

where P_t is the thermal power and dR_t the thermal resistance overcome by the thermal power. To integrate the differential Equation (15) based on Equations (13) and (14), one can write

$$\mathrm{d}R_t = \mathrm{d}R\frac{\sigma}{\lambda} = \frac{\mathrm{d}R}{\lambda\rho} \tag{16}$$

which can also be expressed as

$$\mathrm{d}R = \frac{\mathrm{d}V}{i} \tag{17}$$

Under these conditions, Equation (16) becomes

$$-\lambda\,\rho\,\mathrm{d}T = V\,\mathrm{d}V \tag{18}$$

Equation (18) allows us to express the dependence between the absolute temperature of the contact and the electrical potential, in the form

$$-\int_{T_\Theta}^{T} \lambda\rho \mathrm{d}T = \int_0^V V\mathrm{d}V \tag{19}$$

To solve Equation (19), λ and ρ are considered as functions of temperature. Two cases can arise, namely, the following:

(a) The overtemperature is moderate, i.e., Θ = 1, . . ., 5 degrees. In this case, the product λρ may take an average value $\overline{\lambda\rho}$. Thus, by integrating Equation (19) we obtain

$$T_\Theta - T = \theta_\Theta - \theta = \frac{V^2}{2\overline{\lambda\rho}} \tag{20}$$

and if the integration is performed for a remote area, the contact overtemperature is obtained by

$$T_\Theta - T = \Theta = \frac{U^2}{8\overline{\lambda\rho}} \tag{21}$$

(b) The overtemperature is excessive, meaning that the material tends to melt. In this case, the Wiedemann–Franz–Lorenz law is used,

$$\lambda\rho = LT \tag{22}$$

By integrating within limits T_Θ and T_0 and, respectively, 0 and $U/2$, from Equation (19), we derive

$$L\left(T_\Theta^2 - T_0^2\right) = \frac{U^2}{4} \tag{23}$$

The resistance of the unheated contact (an electric current of zero intensity flows though the contact) differs from the resistance of the heated contact (an electric current of significant intensity flows though it). The dependence between the electrical resistance R_Θ of the heated contact and the electrical resistance R_0 of the unheated contact can be determined using the theory of electric potential. With reference to this, two strictions are considered, namely: striction $S(\lambda, \rho)$, where λ and ρ depend on temperature, and striction $S_0(\lambda_0, \rho_0)$, where λ_0 and ρ_0 do not depend on temperature. For the two strictions, the elementary variation of potential can be expressed as

$$\mathrm{d}V = \rho\frac{\mathrm{d}n}{\Delta A_n}\mathrm{i};\ \mathrm{d}V_0 = \rho_0\frac{\mathrm{d}n}{\Delta A_n}i \tag{24}$$

Since the dependence of resistivity on temperature is of the form $\rho = \rho_0(1 + \alpha_R\theta)$, from Equation (24), it can be written that $\mathrm{d}V = \mathrm{d}V_0(1 + \alpha_R\theta)$, and thus

$$\mathrm{d}V_0 = \mathrm{d}V(1 - \alpha_R\theta) \tag{25}$$

In this case, Equation (19) can also be written as

$$-\int_\Theta^\theta \overline{\lambda\rho}\mathrm{d}\theta = \int_0^V V\mathrm{d}V$$

which becomes, after integration,

$$\theta = \Theta - \frac{1}{2}\cdot\frac{V^2}{\lambda\rho} \tag{26}$$

where, according to (21), $\Theta = \frac{U^2}{8\overline{\lambda\rho}}$.

Equation (25), with the expression of θ introduced from Equation (26), is integrated within limits Θ, 0 for the heating and 0, $U/2$ for the potential:

$$\int_0^{\frac{U_0}{2}} dV_0 = \int_0^{\frac{U}{2}} dV - \int_0^{\frac{U}{2}} \left(\alpha_R \Theta - \frac{\alpha_R V^2}{2\overline{\lambda\rho}} \right) dV$$

or

$$U_0 = U - \alpha_R \Theta U + \frac{\alpha_R U^3}{24\overline{\lambda\rho}} = U\left(1 - \frac{2}{3}\alpha_R \Theta\right) \tag{27}$$

For $\alpha_R \Theta \approx 1$, this can be written as

$$\frac{U}{U_0} = \frac{1}{1 - \frac{2}{3}\alpha_R \Theta} \approx 1 + \frac{2}{3}\alpha_R \Theta \tag{28}$$

Since the current tube of both strictions is traveled by the same current intensity, it can be written as

$$\frac{U}{U_0} = \frac{R_\Theta}{R_0} = 1 + \frac{2}{3}\alpha_R \Theta \tag{29}$$

and finally

$$R_\Theta = R_0\left(1 + \frac{2}{3}\alpha_R \Theta\right) \tag{30}$$

It can therefore be concluded that the resistance of the heated contact can be calculated, starting from the resistance of the unheated contact, with a dependence relationship similar to that of resistors, in which the temperature coefficient of the resistance is 2/3 of the temperature coefficient of the resistivity.

The Thomson effect refers to the case wherein an electric current of intensity i travels through a conductor along which there is a temperature gradient, and additional power develops inside the conductor:

$$P_T = \pm k_T \cdot \Delta T \cdot i \tag{31}$$

where k_T is the Thomson coefficient and ΔT is the temperature difference on the conductor.

The sign ± depends on the direction of current relative to the direction of the temperature gradient. The + sign is considered if the current travels through the conductor in the same direction as the gradient. Current travels through one contact element once in the same direction as the gradient and in the other element in the opposite direction, as shown in Figure 7. As a result, one contact element heats up additionally, and the other cools down. These phenomena manifest themselves in the touch zone, where the temperature is the highest. Accordingly, the anode will be warmer than the cathode.

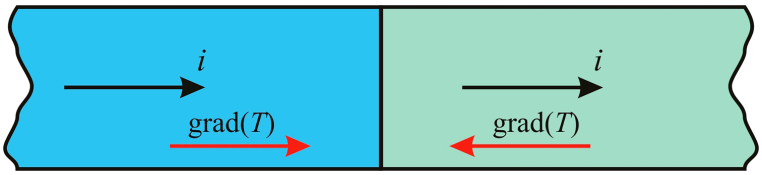

Figure 7. Current travel and the Thomson effect in a contact.

3. Modeling and Simulation of the Electrical Contacts Using Numerical Methods

We have shown in Section 2 that between the absolute temperature of the contacts and their potential, there is a dependence expressed by analytical equations. In order to validate the subsequent numeric simulation, the temperature of the contact was calculated based on the theory shown in the previous section, considering Equation (19), developed for the case of excessive overtemperature, as in Equation (23), considering an electric potential difference of 4 mW. The calculated temperature rise was around 70 degrees, which is within 10–12% of the result obtained by simulation. These equations have a theoretical character, and their resolution by analytical methods is more time consuming than modern numeric

simulation. For this reason, the dependence between the potential and temperature of an electrical contact was analyzed by numerical methods with the aid of the COMSOL Multiphysics software. This is a useful software that allows for running multiple scenarios, with different electric potentials or even using changed contact geometries, in a more facile way as compared to calculations.

3.1. Geometry of the Model

The model of the electrical contact, consisting of an assembly of two contact elements as shown in Figure 8, was built using SolidWorks software. The two elements are identical and the material from which they are built is copper. The geometry and dimensions of one contact element are shown in Figure 9. The advantage of using SolidWorks for building the model is given by the dynamic live link feature it has with COMSOL, meaning that any change to the geometry that is made in SolidWorks is automatically imported into the COMSOL Multiphysics simulation model.

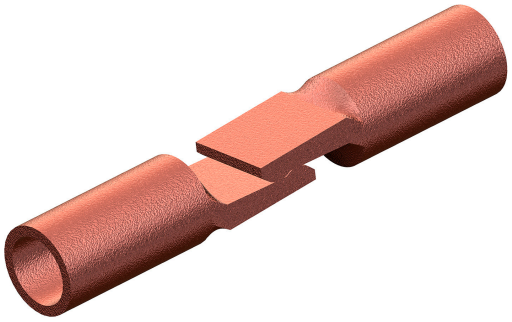

Figure 8. The model of the electrical contact.

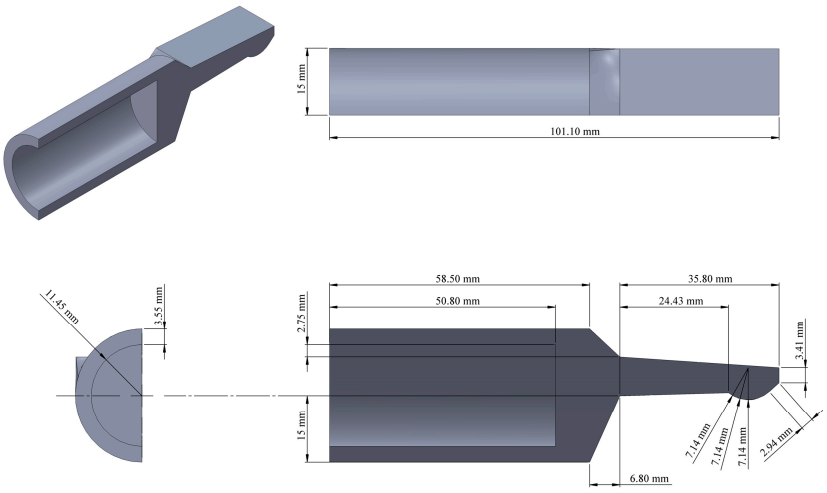

Figure 9. Geometry and dimensions of one contact element.

3.2. The Step-by-Step Simulation Setup for Comsol

The simulation was performed for a 3D model in two distinct steps within stationary studies of Structural Mechanics > Solid Mechanics (solid) and Heat Transfer > Electromagnetic Heating > Joule Heating type.

The two contact elements presented above have a cylindrical body with the touching ends shaped similar to a hook. Here the coupling of apparent thermal and electrical resistances by means of mechanical contact pressure takes place. It was considered that the initial temperature of the contact is equal to the ambient temperature, and the difference of electric potential between the contact elements produces heating by the Joule effect. Figure 10 shows the geometry of the model imported into COMSOL. In the Definitions menu, the Contact Pair type was chosen for

the contact elements and their Source Boundaries and Destination Boundaries were defined as shown in Figure 11.

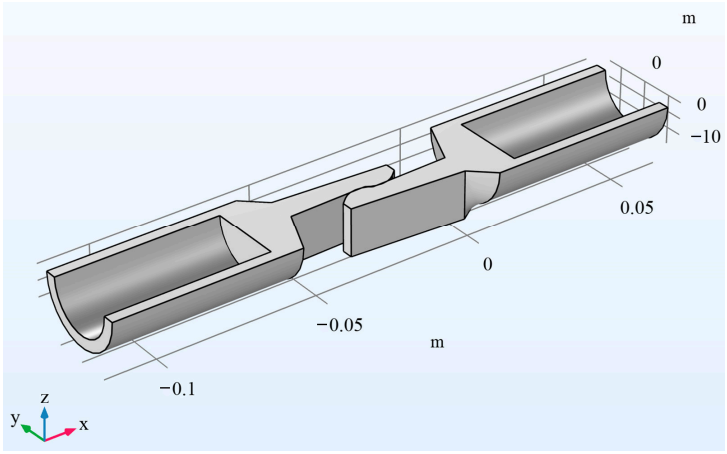

Figure 10. The model geometry as imported into COMSOL.

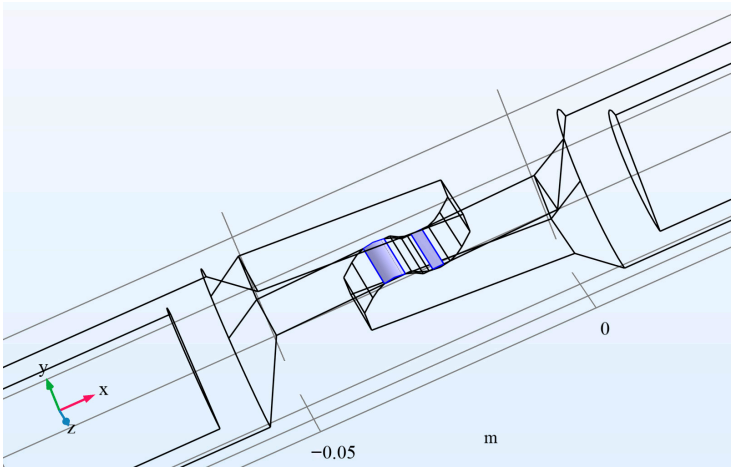

Figure 11. The contact elements, sources and destination boundaries as defined in COMSOL.

Next, for the entire model, the material chosen was copper, with predefined characteristics set in the material library as described in Table 1.

Table 1. Material characteristics of the model.

Property	Variable	Value	Unit
Electrical conductivity	sigma_iso	5.988×10^7	S/m
Heat capacity at constant pressure	Cp	385	J/(kg·K)
Relative permittivity	epsilonr_iso	1	
Density	rho	8960	kg/m^3
Thermal conductivity	k_iso	400	W/(m·K)
Young's modulus	E	110×10^9	Pa
Poisson's ratio	nu	0.35	1
Coefficient of thermal expansion	alpha_iso	17×10^{-6}	1/K
Reference resistivity	rho0	1.72×10^{-8}	Ω·m
Resistivity temperature coefficient	alpha	0.0039	1/K
Reference temperature	Tref	298	K

The fixed surfaces have been established as shown in Figure 12. These surfaces represent the inner part of the semi-cylindrical areas of the contacts. Since the imported geometric pattern is a cross-section through the two electrical contacts, we used the Boundary > Symmetry

option from the Physics menu, and thus the plane of symmetry of the model has been defined (Figure 13). This approach simplifies computations for half of the model.

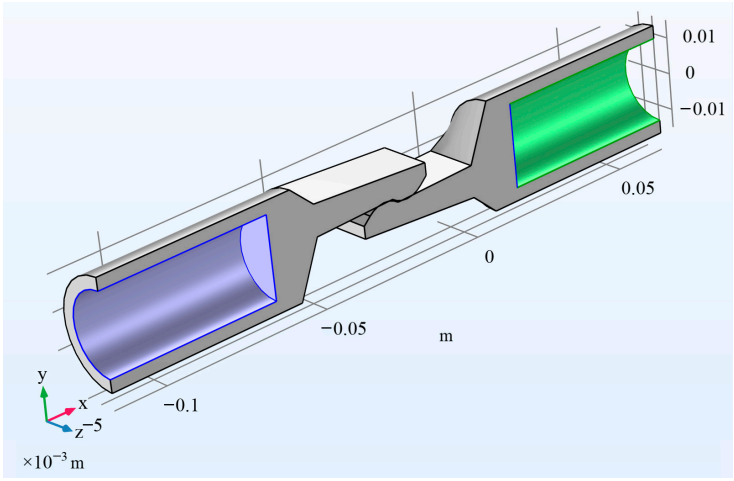

Figure 12. Fixed surfaces definition.

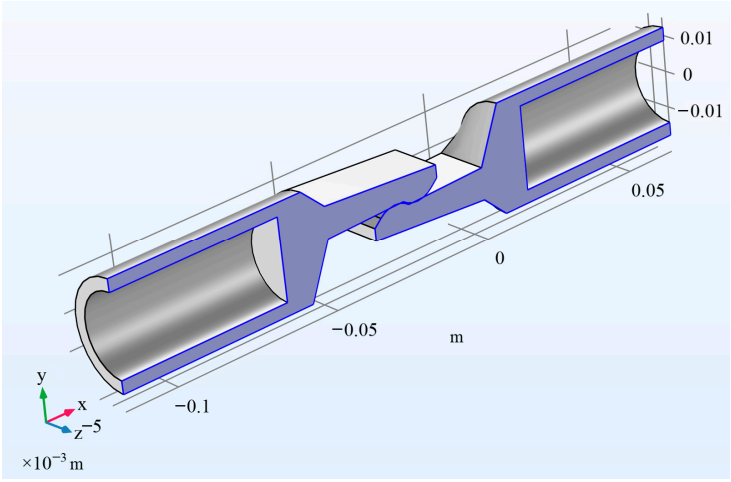

Figure 13. The plane of symmetry for the model.

The contact method was chosen from the COMSOL solver as the Augmented Lagrangian type with the initial value of the contact pressure being $T_n = 1 \times 10^7$ N/m^2. The Augmented Lagrangian method is widely used in simulations involving friction contacts [71], as it is the optimal method of treating constrained minimization problems [72]. Regarding the heat transfer, it was set as Convective heat flux type with a heat transfer coefficient $h = 2$. The difference in electric potential representing the voltage drop on the simulated contact was imposed by assigning zero voltage (ground) to the base surface of the cylinder to one of the contact elements, and a voltage of 1 mV (electric potential) to the other contact element, as shown in Figure 14a,b.

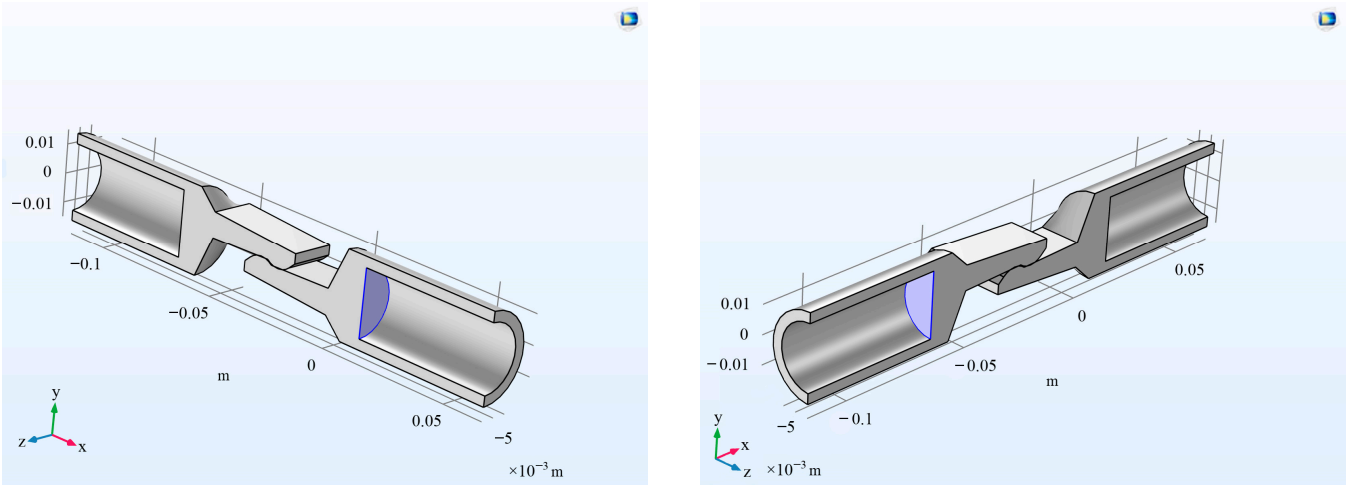

(**a**) (**b**)

Figure 14. (**a**) Contact element with zero voltage (ground). (**b**) Contact element with 1 mV voltage (electric potential).

When modeling using FEA in general (COMSOL in this particular case), it is crucial to select appropriate convergence criteria in order to obtain accurate results. Mesh convergence refers to how small the elements need to be to ensure that the results of the finite element analysis are not affected by changing the size of the mesh. The choice of convergence criteria should be justified based on the specific phenomenon being studied, as well as the chosen model, simulation conditions, and engineer experience. There are two accepted types of methods of refinement for the mesh: the H-based method, where the object is meshed using simple first-order or quadratic elements and the convergence is improved by increasing the elements number, and the P-based method, where the number of elements is kept minimal and the convergence is achieved by increasing the order of the elements. The first case was applied in the present study.

The finite element mesh was defined as the user-controlled mesh type, for which the finite elements size depends on their position in relation to the model, implemented by using the size expression feature offered by the software. Free Tetrahedral type elements were used with the complete mesh consisting of 23,628 tetrahedra, 5208 triangles, 663 edge, and 60 vertex elements. The element volume ratio is 6.388×10^{-3} with an average element quality of 0.6535. The element size as predefined in the general physics setting can take nine values ranging from Extremely Coarse to Extremely Fine. For this simulation, based on the sensitivity test performed, it was determined that the size "Fine" produced consistent and accurate results in a relatively short computing time. The resulting model after meshing based on the data presented is shown in Figure 15.

As stated at the start of Section 3.2, the simulation is carried out in two stages. In the first stage, only solid mechanics phenomena are simulated using the Solid Mechanics (solids) solver, and in the second stage, the Joule effect and heat transfer phenomena are simulated using the Electric Currents and Heat Transfer in Solids solvers. The two stages of the simulation address the need to first solve the effect of the contact pressure on the characteristics of the electrical contact elements material, and next the Joule effect of the contacts.

The simulation of temperature variation when the current flows through the current path of the contact is performed considering an initial temperature of contact elements T = 293.15 K (20 °C). The base values of the parameters for the contact elements were set up prior to the simulation. Thus, in the Solid Mechanics module of Contact Pair 1, the contact pressure was set to $T_n = 1 \times 10^7$ N/m^2. In the Electric Currents > Pair Electrical Contact module, for the same Contact Pair 1, the Microhardness parameter had an assigned value of H_c = 0.1 GPa. In the Heat Transfer in Solids module, an identical value of the microhardness was set for the Thermal Contact pair.

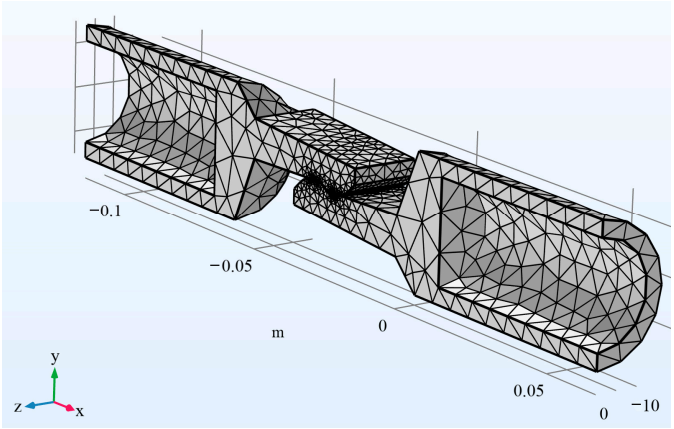

Figure 15. The contact model after finite element meshing.

4. Simulation Results and Discussion

4.1. Results of the Mechanical Simulation

By running the simulation, it has been observed that there is an increase in the von Mises stress (Figure 16a) in the contact where the contact point and the current path are located. A detailed view of the shape of the von Mises stress can be observed in Figure 16b. By analyzing this figure, we can see that the increase in von Mises stress concentrates in the area of physical contact points between the contact elements.

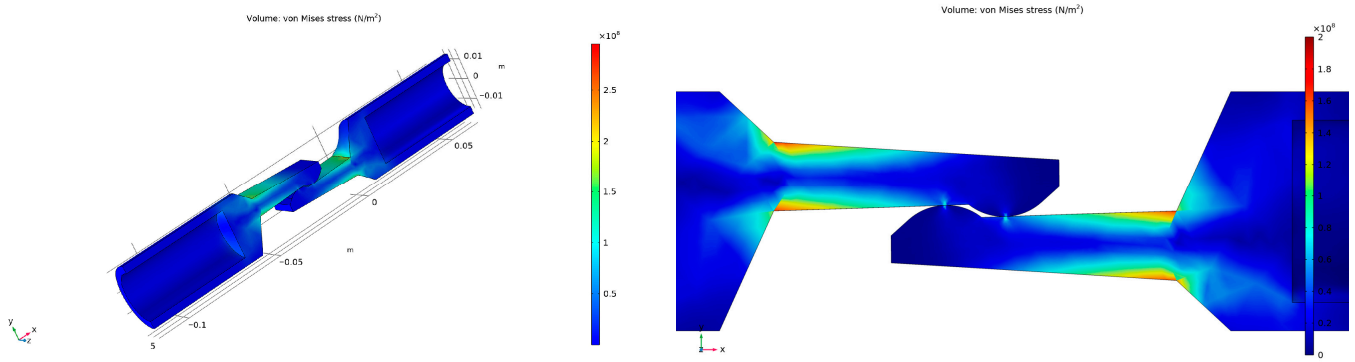

(**a**) (**b**)

Figure 16. (**a**) The von Mises stress in the contact. (**b**) Details of the shape of the von Misses stress at the contact point and the current path location.

The contact forces resulting from the simulation are illustrated in Figure 17 using three-dimensional (17a), detailed (17b), and orthographic (17c) representations.

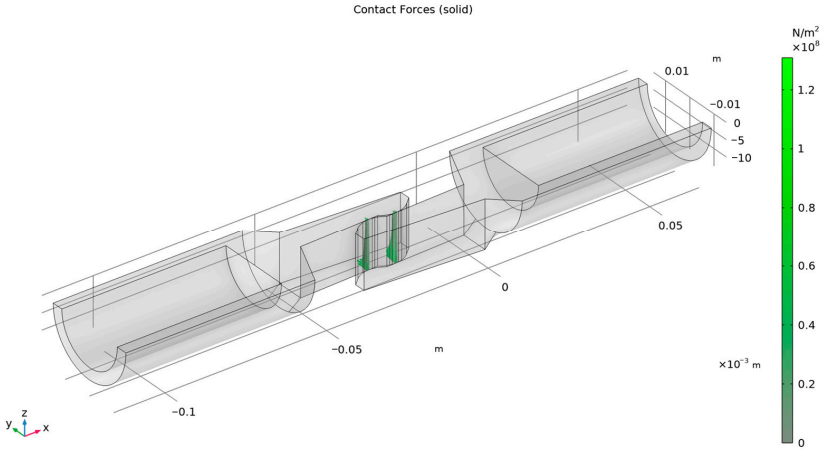

(**a**) Three-dimensional view.

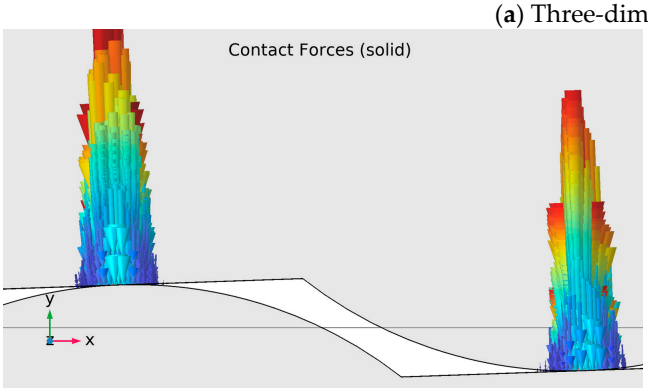

(**b**) Detailed representation.

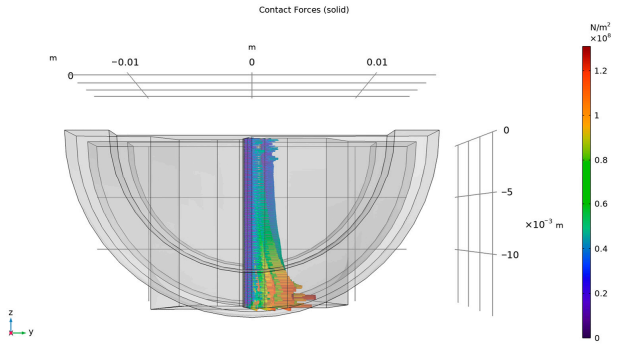

(**c**) Orthographic projection.

Figure 17. The contact forces.

4.2. Results of the Electro-Thermal Simulation

The effects of variations in the electrical potential on the current path of the contact are shown in Figure 18. As expected, they vary between 0 V, which corresponds to the right-hand side element of the contact that is grounded, and 3 mV, corresponding to the left-hand side element. The difference in electric potential is actually the voltage drop in the elements of the electrical contact.

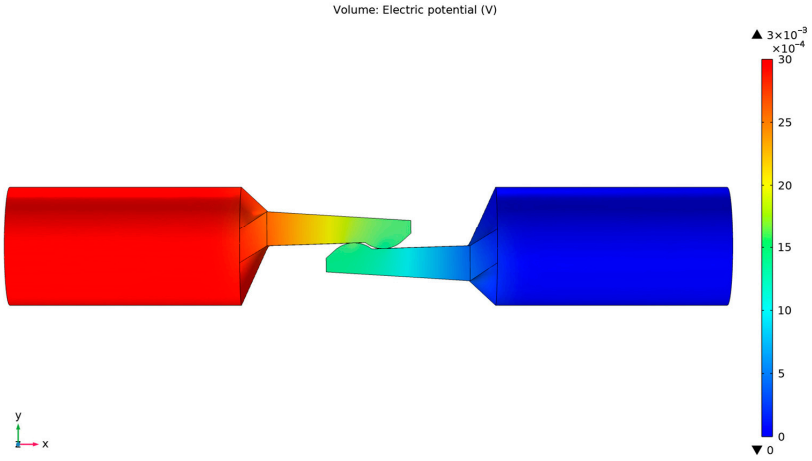

Figure 18. The electrical potential of the contact along the current path.

The variation in the electric field amplitude along the current path is shown in Figure 19a. The Multislice mode combined with the Streamline Multislice mode was used for this repre-

sentation. Figure 19b shows a detail of the variation in the electric field amplitude in the area where the contact elements are touching.

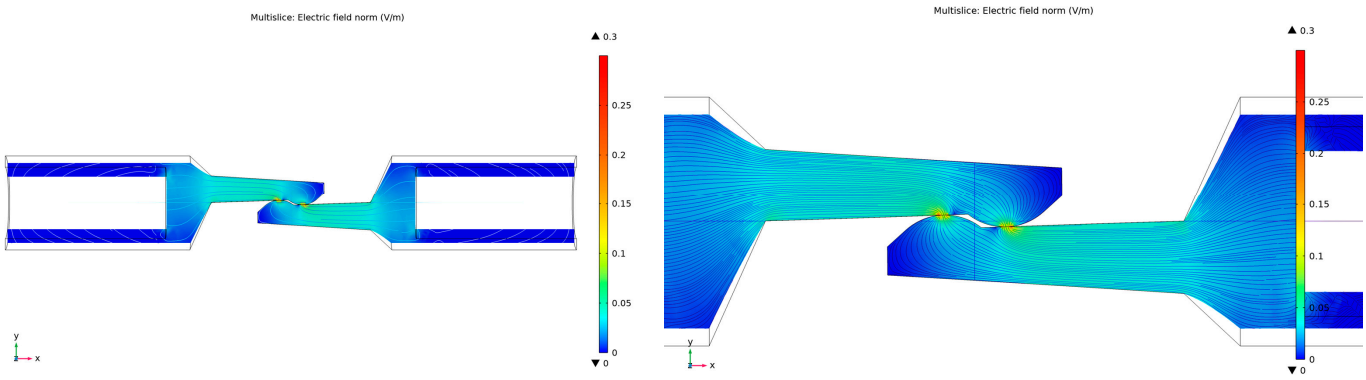

(**a**) (**b**)

Figure 19. (**a**) The variation of the electric field amplitude. (**b**) Details of variation of the electric field amplitude at the touching area.

The variation in the temperature of the current path following the simulation is visible in Figure 20, where one can observe that the highest temperature developed in the touching area of the electrical contact.

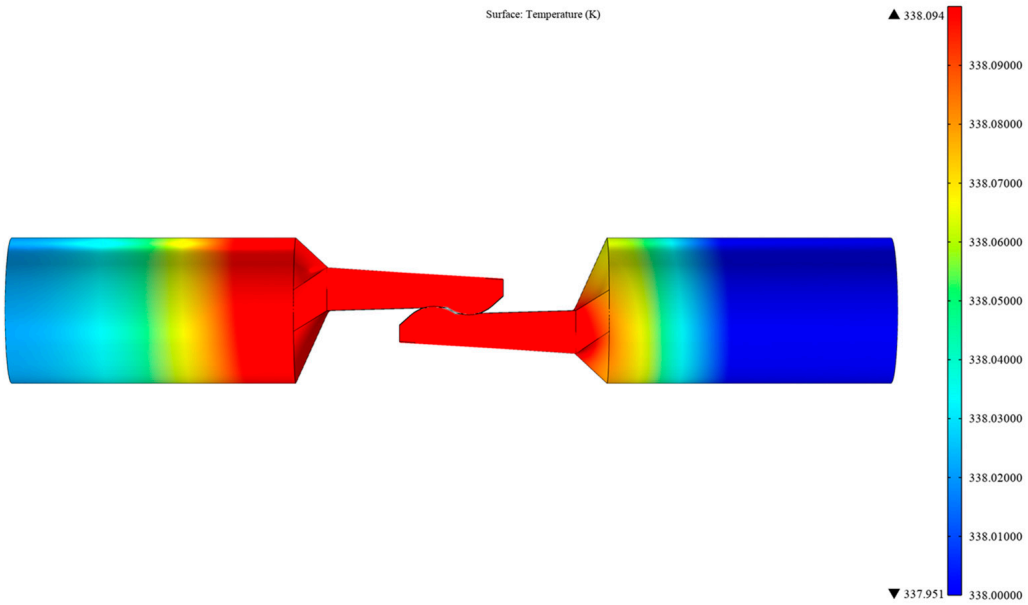

Figure 20. The variation of temperature in the current path and on the contact surface.

Figure 21a shows the simulation results related to the temperature gradient variation along a cut plane passing through the axis of the current path and parallel to plane XY. It can be seen both from the representation of the magnitude of this quantity <K/m> and from the streamline representation that the heat transfer from the element of contact with zero electrical potential is greater than that corresponding to the element of contact with an electric potential of 3 mV.

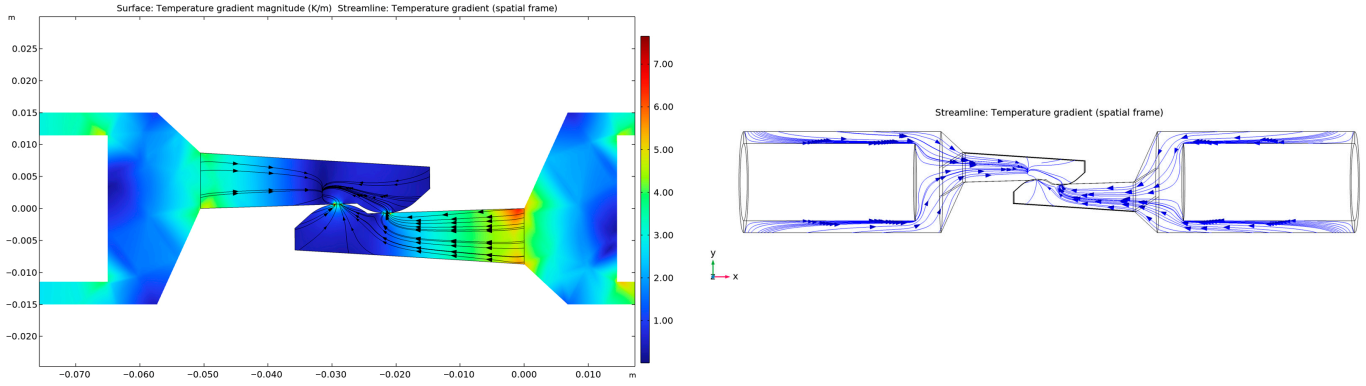

(**a**) (**b**)

Figure 21. (**a**) The temperature gradient's variation along a cutting plane. (**b**) The spatial variation of the temperature gradient along the current path.

Figure 21b shows the spatial variation in the current path's temperature gradient.

Figure 22 shows the temperature variation of the two contact elements and the variation in the current density on a surface that passes through the axis of symmetry of the current path and is parallel to plane XY, using streamline representation.

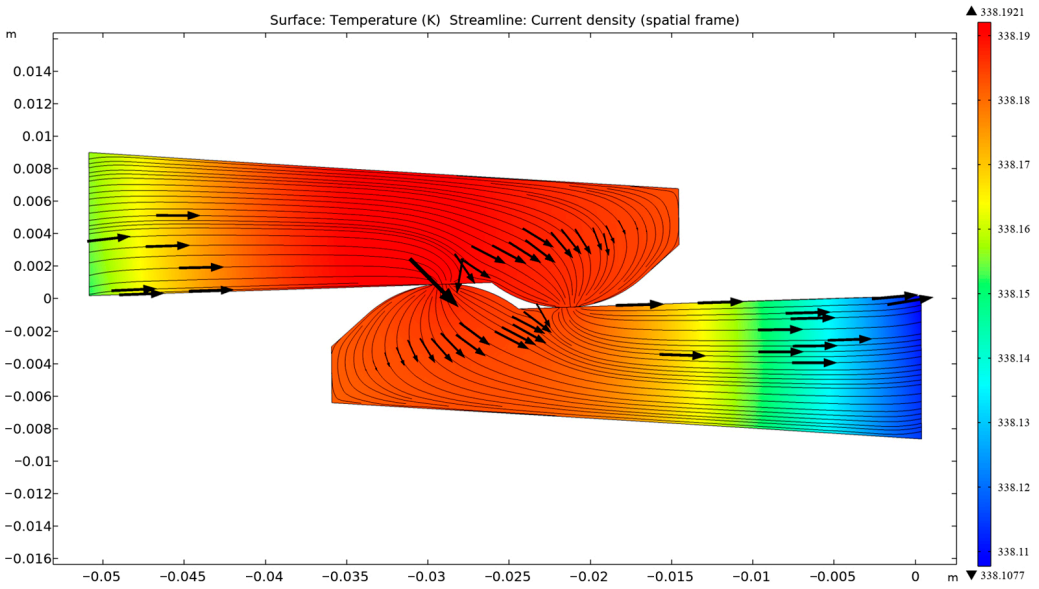

Figure 22. Temperature variation of the contact and the current density using streamlines.

A cut plane was built parallel to plane XZ, passing through the origin of the cartesian coordinate system (Y = 0). Figure 23a,b show the details regarding the positioning of this cut plane.

In Figure 24, the variation in current density on the cut plane defined above is presented. In Figure 25, the variation in the current density is shown using a three-dimensional representation and a Max/Min-Point diagram showing the density of electric energy. One can see that the highest density of electric energy developed at the touching area of the contact elements.

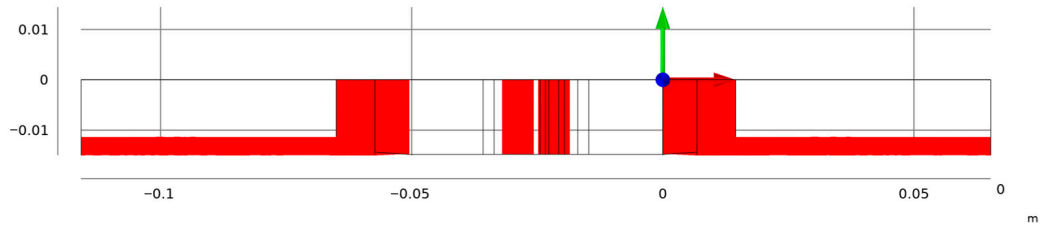

(**a**) Cut plane top view.

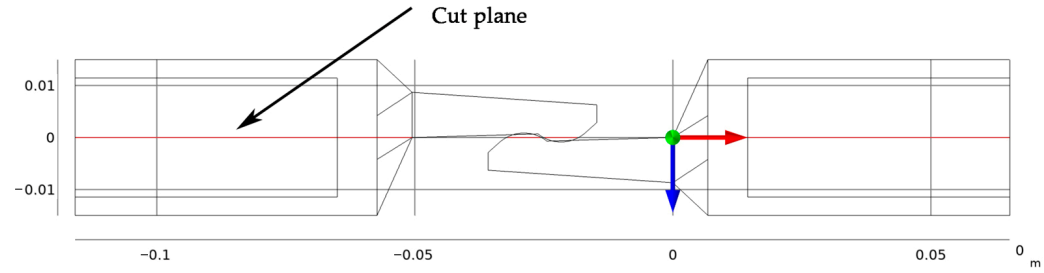

(**b**) Cut plane side view.

Figure 23. Cut plane building and details on its positioning.

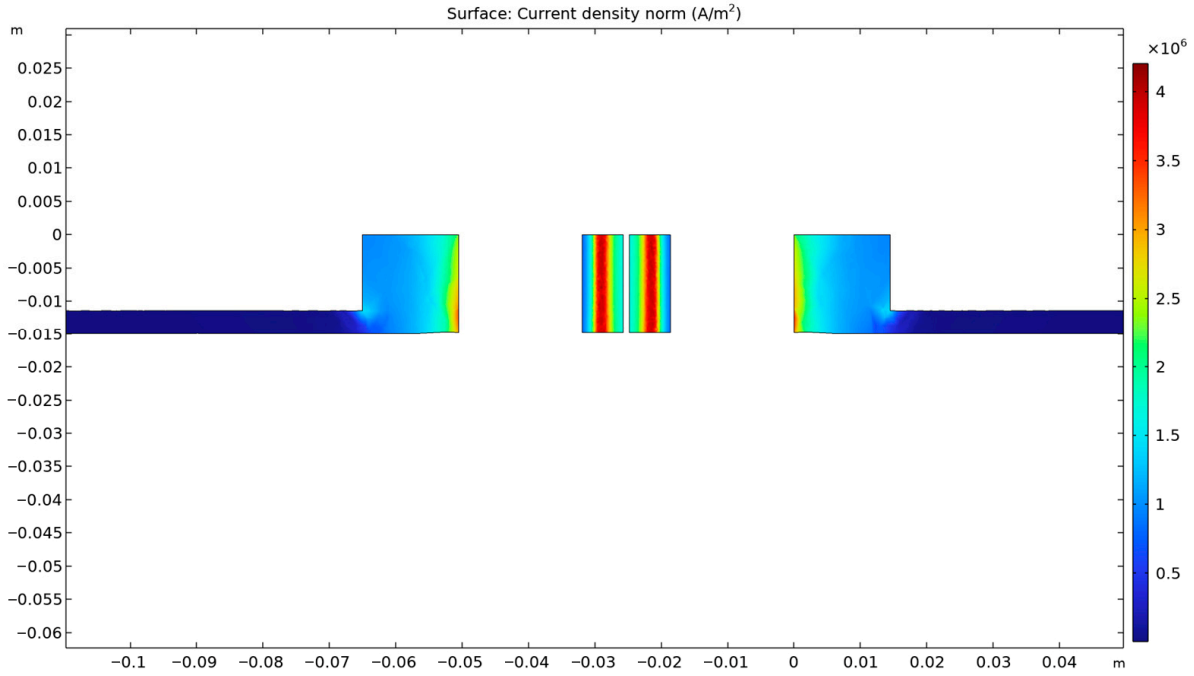

Figure 24. Variation in the current density on the cut plane.

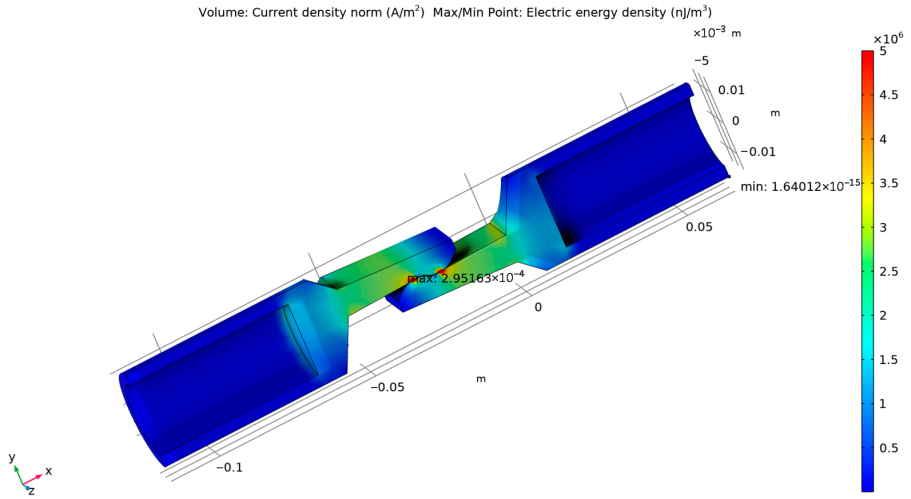

Figure 25. Variation in the current density at the contact (3D), and the Max/Min-Point diagram of the electric energy density.

A dataset element of the type Edge 3D was created (see in Figure 26) along an edge line of one contact element in order to plot the temperature variation along this edge, as presented in Figure 27.

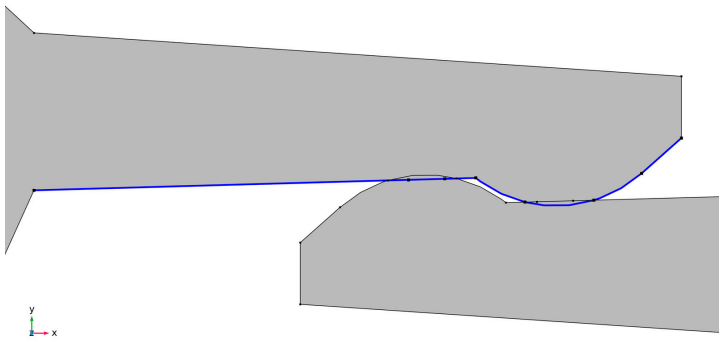

Figure 26. Edge 3D-type dataset created for the edge of a contact element.

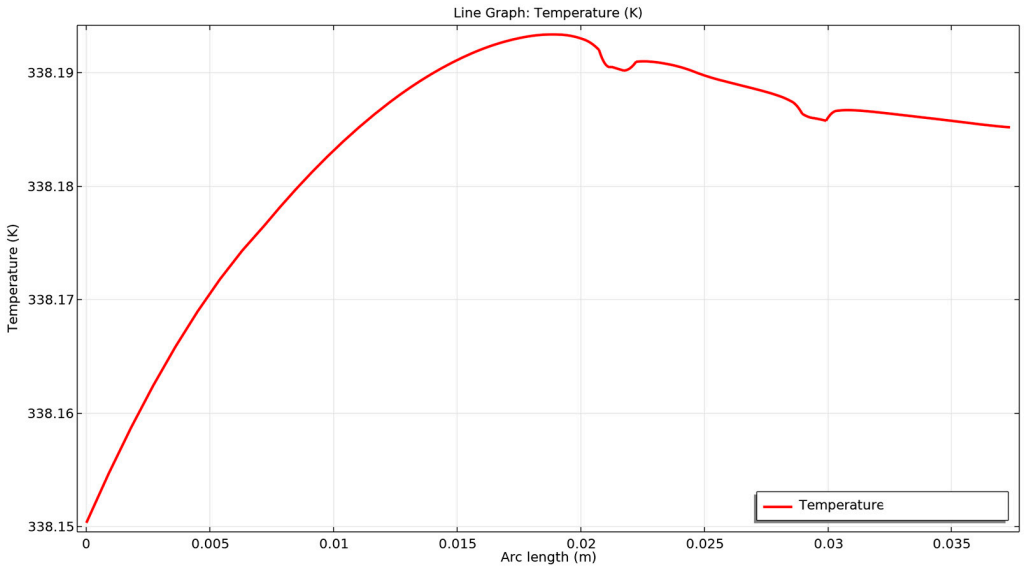

Figure 27. Variation of the temperature along the contact element edge.

In a similar way, two Edge 3D type datasets have been created (Figure 28a,b) for the contours of both electrical contact elements, to be used for the plotting of the variation graph of the electrical potential, as shown in Figure 29.

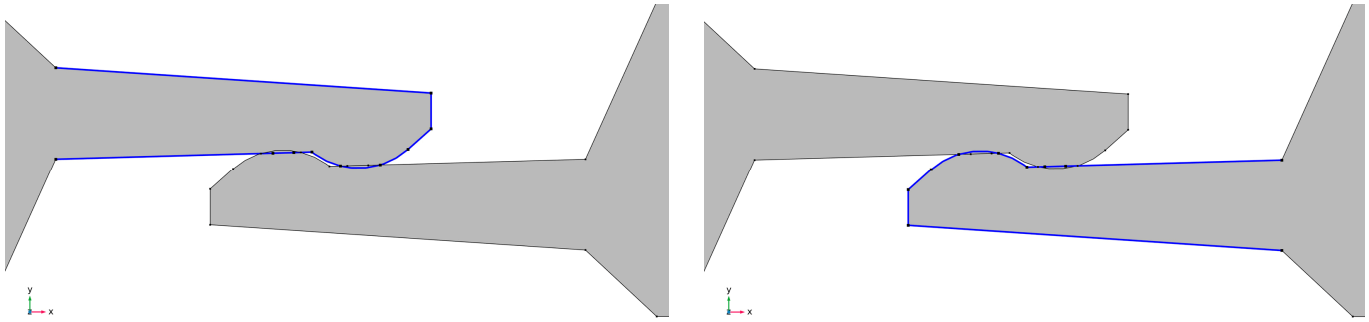

(**a**) (**b**)

Figure 28. The two Edge 3D datasets created for the contours of: (**a**) Top contact element. (**a**) Bottom contact element.

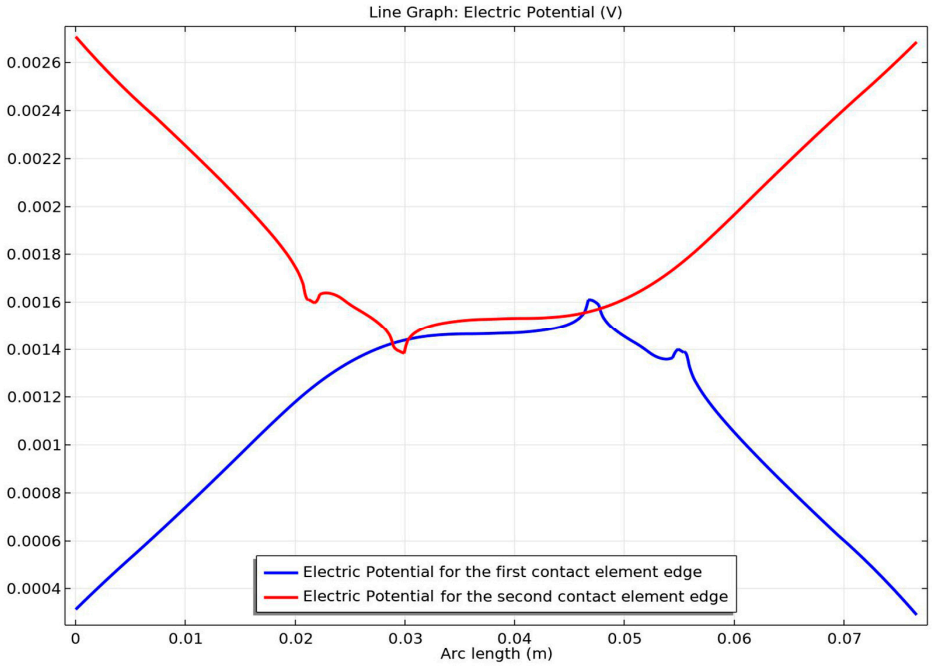

Figure 29. Variation of the electric potential along the two contact element edges.

In order to highlight the variation in the maximum temperature of the current path and its dependence on the value of the contact voltage, the simulations were run for various values of the potential difference between the two elements of the electrical contact. These data, the values of the maximum temperature, and the values of the temperature increase as compared to the ambient temperature are all summarized in Table 2.

Table 2. Temperature increase function of the contact voltage resulting from simulations.

Electric Potential (Contact Voltage) Difference [mV]	Maximum Contact Temperature		Temperature Variation (Increase) [ΔT]
	[K]	[°C]	
Ambient temperature T = 293.15 K/20 °C			
0	293.15	20.00	0.00
0.50	294.28	21.13	1.13
1.00	298.07	24.92	4.92
2.00	312.93	39.78	19.78
3.00	337.65	64.50	44.50
4.00	372.39	99.25	79.25
5.00	416.96	143.81	123.81

The variation in the temperature as a function of the contact voltage values is plotted in Figure 30. As one can observe, the red curve representing this variation has a parabolic shape. A trendline curve of polynomial type 2 represented in black was also traced, with its equation displayed. This trendline overlaps the curve of the variation in the temperature increase.

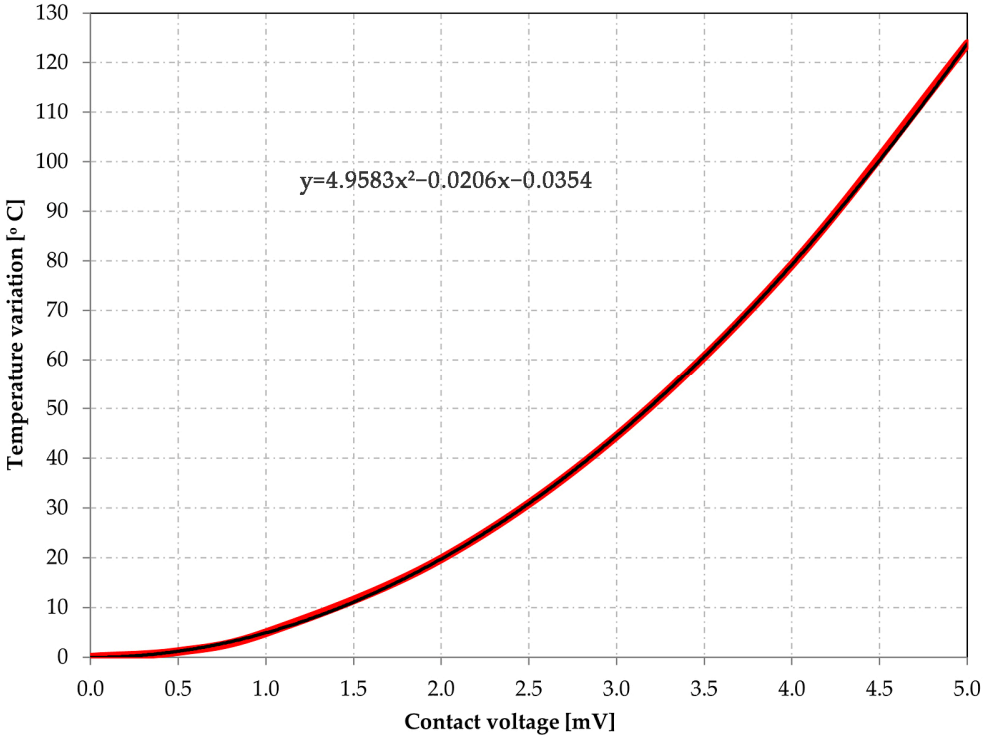

Figure 30. Variation of the temperature as a function of the contact voltage.

5. Conclusions

The present paper studies and highlights—using numerical methods of modeling and simulation offered by COMSOL Multiphysics software (specifically three of its simulation modules: solid state mechanics module, electric current module and heat transfer module)—the dependence between the contact voltage (the voltage drop on the contact) and the variation in its temperature, but also in the current path within the contact.

The results obtained after the simulations show that, from a mechanical point of view, the maximum value of the contact force is found at the points of contact, and the von Misses stress takes higher values in the current path area where the flat part intersects with the cylindrical shape for each contact element, and also in the area of the physical touching of the two contact elements.

From electro-thermal points of view, the theoretical aspects presented in the Introduction section and shown in Figure 7 are proven by the graphical representation of temperature gradient along the contact, where the highest temperature occurs in the touching area and the gradient increases in the direction from the zero potential contact elements towards the contact point. Also, various representations (on a plane of symmetry, and using streamlines) were plotted for the dependence between the temperature variation of the contact elements and the variation of the current density. Finally, temperature variation diagrams along the edges of the contacts were traced to highlight the maximum values.

The maximum contact temperature values were computed by simulation for contact voltages between 0 and 5 mV. Thus, the curve of variation of the increase in contact temperature relative to the contact temperature was plotted, finding this variation to be parabolic.

The study of the obtained values during simulations indicates an undesirable increase in contact temperature for values higher than 4 mV of voltage drop, with temperatures that may affect the integrity of insulating materials in the electrical contact. This finding is important, as damage to the insulation materials may cause the phenomenon of overturning, or short-circuiting in the electrical contact devices, thus leading to fire and damage.

The analysis of these aspects can constitute a future direction of research. Another future direction of research could be the extension of the study to analyze contact behavior not only for the static stresses implied by the normal closing of contact, but also considering dynamic mechanical stresses induced by shock or vibration. A third possible development of this study could be an experimental study and the comparison of its findings to the results of numerical simulation.

Author Contributions: All authors have contributed to the preparation of this manuscript. Conceptualization, A.A., F.D.P. and D.P.; methodology, S.M.R., A.A., I.B. and M.A.R.; software, F.D.P., A.A., and D.P.; writing—original draft preparation, S.M.R., F.D.P. and A.A.; writing—review and editing, D.P., M.A.R., I.B. and D.P. All authors have read and agreed to the published version of the manuscript.

Funding: This research received no external funding.

Institutional Review Board Statement: Not applicable.

Informed Consent Statement: Not applicable.

Data Availability Statement: Data are contained within the article.

Conflicts of Interest: The authors declare no conflicts of interest.

References

1. Johnson, K.L. *Contact Mechanics*; Cambridge University Press: Cambridge, UK, 1985. [CrossRef]
2. Braunovic, M.; Myshkin, N.K.; Konchits, V. *Electrical Contacts: Fundamentals, Applications and Technology*; CRC Press: Boca Raton, FL, USA, 2006. [CrossRef]
3. Popov, V.L. *Contact Mechanics and Friction*; Springer: Berlin/Heidelberg, Germany, 2017. [CrossRef]
4. Slade, P.G. *Electrical Contacts: Principles and Applications*, 2nd ed.; CRC Press: London, UK, 2017. [CrossRef]
5. Barber, J.R. *Contact Mechanics*, 1st ed.; Springer: Berlin, Germany, 2018.
6. Zhou, X. Electric Contact, Elements, and Systems. In *Encyclopedia of Tribology*; Wang, Q.J., Chung, Y.W., Eds.; Springer: Boston, MA, USA, 2013. [CrossRef]
7. Persson, B.N.J. On the Electric Contact Resistance. *Tribol. Lett.* **2022**, *70*, 88. [CrossRef]
8. Müser, M.H.; Wang, A. Contact-patch-size distribution and limits of self-affinity in contacts between randomly rough surfaces. *Lubricants* **2018**, *6*, 85. [CrossRef]
9. Prodanov, N.; Dapp, W.B.; Müser, M.H. On the contact area and mean gap of rough, elastic contacts: Dimensional analysis, numerical corrections, and reference data. *Tribol. Lett.* **2014**, *53*, 433. [CrossRef]
10. Qiu, D.; Peng, L.; Yi, P.; Lai, X. A micro contact model for electrical contact resistance prediction between roughness surface and carbon fiber paper. *Int. J. Mech. Sci.* **2017**, *124*, 37–47. [CrossRef]
11. He, L.P.; Cai, Z.B.; Peng, J.F.; Deng, W.L.; Li, Y.; Yang, L.Y.; Zhu, M.H. Effects of oxidation layer and roughness on the fretting wear behavior of copper under electrical contact. *Mater. Res. Express* **2020**, *6*, 1265e3. [CrossRef]
12. Zhang, C.; Ren, W.; Liao, X. On the Relationship between Contact Resistance and Load Force for Electrode Materials with Rough Surfaces. *Materials* **2022**, *15*, 5667. [CrossRef] [PubMed]

13. Biele, L.; Schaaf, P.; Schmid, F. Influence of Contact Pressure on the Specific Electrical Contact Resistance of Copper. *IEEE Trans. Compon. Packag. Manuf. Technol.* **2022**, *12*, 973–980. [CrossRef]
14. Timsit, R.S. Electrical Contacts: Scientific Fundamentals. In *Encyclopedia of Tribology*; Wang, Q.J., Chung, Y.W., Eds.; Springer: Boston, MA, USA, 2013. [CrossRef]
15. Faltin, C. Exact solution of constriction resistance and temperature field within a homogeneous cylindrical body heated by an isothermal circular contact spot. *Int. Commun. Heat Mass Transf.* **1985**, *12*, 677–686. [CrossRef]
16. Negus, K.J.; Yovanovich, M.M.; Beck, J.V. On the nondimensionalization of constriction resistance for semi-infinite heat flux tubes. *J. Heat Transf.* **1989**, *111*, 804–807. [CrossRef]
17. Yovanovich, M.M. Overall constriction resistance between contacting rough, wavy surfaces. *Int. J. Heat Mass Transf.* **1969**, *12*, 1517–1520. [CrossRef]
18. Lambert, M.A.; Fletcher, L.S. Thermal contact conductance of spherical rough metals. *J. Heat Transf.* **1997**, *119*, 684–690. [CrossRef]
19. Lei, H.; Zhu, X.; Wang, H.; Chen, J.; Liu, Q.; Niu, C.; Wang, L.; Yang, F. Investigation on Mathematical Model of Electric Contact Based on Fractal Geometry. *Lect. Notes Electr. Eng.* **2021**, *742*, 617–628. [CrossRef]
20. Capelli, F.; Riba, J.-R.; Rupérez, E.; Sanllehí, J. A Genetic-Algorithm-Optimized Fractal Model to Predict the Constriction Resistance From Surface Roughness Measurements. *IEEE Trans. Instrum. Meas.* **2017**, *66*, 2437–2447. [CrossRef]
21. Zou, M.; Yu, B.; Cai, J.; Xu, P. Fractal model for thermal contact conductance. *J. Heat Transf.* **2008**, *130*, 101301. [CrossRef]
22. Talukder, S.; Yeo, C.-D.; Hong, Y.-K.; Choi, M.; Flicek, R.C.; Bishop, J.E. Analytical modeling and simulation of electrical contact resistance for elastic rough electrode surface contact including frictional temperature rise. *AIP Adv.* **2022**, *12*, 025204. [CrossRef]
23. Popescu, A.; Lazarescu, E.; Frigura-Iliasa, F.M.; Dolga, L.; Filipescu, H.E.; Andreea, A. Analytical Model for the Electrodynamical Forces inside Electrical Contacts of Commutation Devices. In Proceedings of the 2019 20th International Scientific Conference on Electric Power Engineering (EPE), Kouty nad Desnou, Czech Republic, 15–17 May 2019; pp. 1–4. [CrossRef]
24. Shah, S.G.; Krithivasan, V.; Jackson, R.L. An electro-mechanical contact analysis of a three-dimensional sinusoidal surface against a rigid flat. *Wear* **2011**, *270*, 914–921. [CrossRef]
25. Blauth, M.; Berger, F.; Song, J. Analytical and Experimental Investigation of the Electrical-Thermal Behaviour of Electrical Contact Systems. *Br. J. Appl. Sci. Technol.* **2014**, *4*, 18–39. [CrossRef]
26. Dutta, S.; Vikram, G.N.V.R.; Bobji, M.S.; Mohan, S. Table top experimental setup for electrical contact resistance measurement during indentation. *Measurement* **2020**, *152*, 107286. [CrossRef]
27. Kogut, L.; Komvopoulos, K. Analysis of interfacial adhesion based on electrical contact resistance measurements. *J. Appl. Phys.* **2003**, *94*, 6386–6390. [CrossRef]
28. Beloufa, A. Numerical and experimental optimization of mechanical stress, contact temperature and electrical contact resistance of power automotive connector. *Int. J. Mech.* **2010**, *4*, 94–104.
29. Zhang, S.; Zhao, X.; Ye, M.; He, Y. Theoretical and Experimental Study on Electrical Contact Resistance of Metal Bolt Joints. *IEEE Trans. Compon. Packag. Manuf. Technol.* **2019**, *9*, 1301–1309. [CrossRef]
30. Pradille, C.; Bay, F.; Mocellin, K. An Experimental Study to Determine Electrical Contact Resistance. In Proceedings of the 56th IEEE Holm Conference on Electrical Contacts, Charleston, SC, USA, 4–7 October 2010; pp. 1–5. [CrossRef]
31. Wangwiwattana, S.; Yoshikazu, K. Joule Heating and Arc-Fault-Induced Electrical Fires for Commercial-Grade Copper and Brass in Low-Voltage Electrical Systems. *Appl. Sci.* **2022**, *12*, 4710. [CrossRef]
32. Zavarise, G.; Wriggers, P.; Stein, E.; Schrefler, B.A. Real contact mechanisms and finite element formulation—A coupled thermomechanical approach. *Int. J. Numer. Methods Eng.* **1992**, *35*, 767–785. [CrossRef]
33. Wriggers, P.; Miehe, C. Contact constraints within coupled thermomechanical analysis-a finite element model. *Comput. Methods Appl. Mech. Eng.* **1994**, *113*, 301–319. [CrossRef]
34. Zienkiewicz, O.C.; Taylor, R.L. *The Finite Element Method*, 4th ed.; McGraw-Hill: London, UK, 1989.
35. Agelet de Saracibar, C. Numerical analysis of coupled thermomechanical frictional contact problems. Computational model and applications. *Arch. Comput. Methods Eng.* **1998**, *5*, 243–301. [CrossRef]
36. Weißenfels, C.; Wriggers, P. Numerical modeling of electrical contacts. *Comput. Mech.* **2010**, *46*, 301–314. [CrossRef]
37. Renouf, M.; Fillot, N. Coupling electrical and mechanical effects in discrete element simulations. *Int. J. Numer. Methods Eng.* **2007**, *74*, 238–254. [CrossRef]
38. Bourbatache, K.; Guessasma, M.; Bellenger, E.; Bourny, V.; Tekaya, A. Discrete modelling of electrical transfer in multi-contact systems. *Granul. Matter* **2012**, *14*, 1–10. [CrossRef]
39. Zhang, J.; Zavaliangos, A. Discrete element simulation of transient hermos-electrical phenomena in particulate system. In *Granular Material-Based Technologies*; MRS Proceedings: Boston, MA, USA, 2002; Volume 759.
40. Fortin, J.; Millet, O.; De Saxcè, G. Numerical simulation of granular materials by an improved discrete element method. *Int. J. Numer. Methods Eng.* **2004**, *62*, 639–663. [CrossRef]
41. Gwinner, J.; Stephan, E.P. BEM for Contact Problems. In *Advanced Boundary Element Methods. Springer Series in Computational Mathematics*; Springer: Cham, Switzerland, 2018; Volume 52, pp. 389–449. [CrossRef]
42. Frérot, L.; Bonnet, M.; Molinari, J.-F.; Anciaux, G. A Fourier-accelerated volume integral method for elastoplastic contact. *Comput. Methods Appl. Mech. Eng.* **2019**, *351*, 951–976. [CrossRef]
43. Xu, Y.; Jackson, R.L. Boundary element method (BEM) applied to the rough surface contact vs. BEM in computational mechanics. *Friction* **2018**, *7*, 359–371. [CrossRef]

44. Szulborski, M.; Łapczyński, S.; Kolimas, Ł.; Zalewski, D. Transient Thermal Analysis of the Circuit Breaker Current Path with the Use of FEA Simulation. *Energies* **2021**, *14*, 2359. [CrossRef]
45. Zhang, C.; Ren, W.; Wang, G.A. Finite Element Method to Investigate Electrical Contact Behaviors Considering Asperity Interactions. In Proceedings of the 2020 IEEE 66th Holm Conference on Electrical Contacts and Intensive Course (HLM), San Antonio, TX, USA, 30 September–7 October 2020; pp. 98–104. [CrossRef]
46. Riba, J.-R.; Mancini, A.-G.; Abomailek, C.; Capelli, F. A 3D-FEM-based model to predict the electrical constriction resistance of compressed contacts. *Measurement* **2018**, *114*, 44–50. [CrossRef]
47. Li, Y.-H.; Shen, F.; Ke, L.-L. Multi-physics electrical contact analysis considering the electrical resistance and Joule heating. *Int. J. Solids Struct.* **2022**, *256*, 111975. [CrossRef]
48. Shen, F.; Ke, L.-L. Numerical Study of Coupled Electrical-Thermal-Mechanical-Wear Behavior in Electrical Contacts. *Metals* **2021**, *11*, 955. [CrossRef]
49. Gonzalo, S.R. Coupling of Mechanical and Electrical Contact Behavior of Current Carrying Connections in Finite element Models. Bachelor's Thesis, Universidad de Valladolid, Escuela de Ingenierías Industriales, Valladolid, Spain, 2021.
50. Hamdia, K.M. A representative volume element model to evaluate the effective properties of flexoelectric nanocomposite. *Eur. J. Mech. A/Solids* **2023**, *103*, 105149. [CrossRef]
51. Angadi, S.V.; Jackson, R.L.; Pujar, V.V.; Tushar, M. A Comprehensive Review of the Finite Element Modeling of Electrical Connectors Including Their Contacts. *IEEE Trans. Compon. Packag. Manuf. Technol.* **2020**, *10*, 836–844. [CrossRef]
52. Kim, S.H.; Lee, K.W. Numerical approach to joule heating analysis for electrical parts using MSC Marc. *J. Mech. Sci. Technol.* **2015**, *29*, 2081–2087. [CrossRef]
53. Lv, B.; Zhou, S.J.; Zhao, L.Y. Technical research on optimization design of contacts of electrical connector. *J. Zhejiang Univ. -Sci. A* **2007**, *8*, 506–510. [CrossRef]
54. Duan, K.; Zhu, F.; Li, Y.; Tang, K.; Liu, S.; Chen, Y. Contact resistance investigation of electrical connector with different shrink range. In Proceedings of the 2014 15th International Conference on Electronic Packaging Technology, Chengdu, China, 12–15 August 2014; pp. 1146–1149. [CrossRef]
55. Liu, H.; Leray, D.; Pons, P.; Colin, S. Finite element multi-physics modeling for ohmic contact of microswitches. In Proceedings of the 15th International Conference on Thermal, Mechanical and Mulit-Physics Simulation and Experiments in Microelectronics and Microsystems (EuroSimE), Ghent, Belgium, 7–9 April 2014; pp. 1–8. [CrossRef]
56. Angadi, S.V.; Wilson, W.E.; Jackson, R.L.; Flowers, G.; Rickett, B. A Multi-Physics Finite Element Model of an Electrical Connector Considering Rough Surface Contact. In Proceedings of the 2008 IEEE 54th Holm Conference on Electrical Contacts, Orlando, FL, USA, 27–29 October 2008; pp. 168–177. [CrossRef]
57. Luo, S.; Wang, B.; Jiang, J.; Li, J.; Zou, G.; Zeng, L. Numerical analysis on mechanical and fatigue behaviors of aviation electrical connector considering structural effect. *Int. J. Numer. Model. Electron. Netw. Devices Fields* **2024**, *37*, e3183. [CrossRef]
58. Ren, W.B.; Cui, L.; Zhai, G. Simulation of contacts inserted characteristics and contact resistance for electrical connector. *J. Electromechanical Compon.* **2012**, *32*, 40–48.
59. Terhorst, M.; Ozhoga-Maslovskaja, O.; Trauth, D.; Shirobokov, A.; Mattfeld, P.; Solf, M.; Klocke, F. Electro-thermo-mechanical contact model for bulk metal forming under application of electrical resistance heating. *Int. J. Adv. Manuf. Technol.* **2017**, *89*, 3601–3618. [CrossRef]
60. Zhang, J.; Huang, L.; Chen, T.; Su, G. Simulation based analysis of electrical fire risks caused by poor electric contact between plug and receptacle. *Fire Saf. J.* **2021**, *126*, 103434. [CrossRef]
61. Guo, F.; Gu, X.; Li, L.; Wang, Z.; Wang, T.; Jia, S. Effect of surface microparameters on contact temperature of sliding electrical contact. *IEEE Trans. Ind. Inform.* **2021**, *18*, 5972–5981. [CrossRef]
62. Zhang, C.; Zhao, Z.; Ren, W. Simulation and experimental investigation of contact spot temperature for electrical contact components. *IOP Conf. Ser. Mater. Sci. Eng.* **2021**, *1207*, 012021. [CrossRef]
63. Andras, A.; Brînas, I.; Radu, S.M.; Popescu, F.D.; Popescu, V.; Budilica, D.I. Investigation of the Thermal Behaviour for the Disc-Pad Assembly of a Mine Hoist Brake Using COMSOL Multiphysics. *Acta Tech. Napoc. Ser. Appl. Math. Mech. Eng.* **2021**, *64*, 227–234.
64. Popescu, F.D.; Radu, S.M.; Andraș, A.; Brînaș, I.; Budilică, D.I.; Popescu, V. Comparative Analysis of Mine Shaft Hoisting Systems' Brake Temperature Using Finite Element Analysis (FEA). *Materials* **2022**, *15*, 3363. [CrossRef] [PubMed]
65. Popescu, F.D.; Radu, S.M.; Andraş, A.; Brînaş, I.K. A Grafo-Numeric Method of Determination of the Operation Power of the Rotor of EsRc-1400 Bucket Wheel Excavator Using Computer Simulation in SolidWorks. *MATEC Web Conf.* **2019**, *290*, 04007. [CrossRef]
66. Popescu, F.D.; Radu, S.M.; Andras, A.; Brinas, I.; Marita, M.-O.; Radu, M.A.; Brinas, C.L. Stability Assessment of the Dam of a Tailings Pond Using Computer Modeling—Case Study: Coroiești, Romania. *Appl. Sci.* **2024**, *14*, 268. [CrossRef]
67. COMSOL. *COMSOL Multiphysics 5.3. Reference Manual*; COMSOL AB: Stockholm, Sweden, 2017.
68. Zhai, C.; Hanaor, D.; Proust, G.; Gan, Y. Stress-dependent electrical contact resistance at fractal rough surfaces. *J. Eng. Mech.* **2017**, *143*, B4015001. [CrossRef]
69. Holm, R. *Electric Contacts: Theory and Application*; Springer Science & Business Media: New York, NY, USA, 2013.
70. Hortopan, G. *Aparate Electrice. Principii și Aplicații*; Editura Didactică și Pedagogică: București, Romania, 1980.

71. Simo, J.C.; Laursen, T.A. An augmented lagrangian treatment of contact problems involving friction. *Comput. Struct.* **1992**, *42*, 97–116. [CrossRef]
72. Pennec, F.; Achkar, H.; Peyrou, D.; Plana, R.; Pons, P.; Courtade, F. Verification of Contact Modeling with COMSOL Multiphysics Software. In Proceedings of the Federation of European Simulation Societies Conference (EUROSIM), Ljubljana, Slovenia, 9–13 September 2007.

Disclaimer/Publisher's Note: The statements, opinions and data contained in all publications are solely those of the individual author(s) and contributor(s) and not of MDPI and/or the editor(s). MDPI and/or the editor(s) disclaim responsibility for any injury to people or property resulting from any ideas, methods, instructions or products referred to in the content.